Test of validity of the *V*-type approach for electron trajectories in reflection electron energy loss spectroscopy

F. Yubero,[1] N. Pauly,[2] A. Dubus,[2] and S. Tougaard[3]
[1]*Instituto de Ciencia de Materiales de Sevilla (CSIC-Univ. Sevilla), C/Américo Vespucio 49, E-41092 Sevilla, Spain*
[2]*Université Libre de Bruxelles, Service de Métrologie Nucléaire, Code Postal 165/84, 50 Avenue, F. D. Roosevelt, B-1050 Brussels, Belgium*
[3]*Department of Physics and Chemistry, University of Southern Denmark, DK-5230 Odense M, Denmark*
(Received 30 October 2007; revised manuscript received 3 January 2008; published 4 June 2008)

An electron reaching the detector after being backscattered from a solid surface in a reflection electron energy loss spectroscopy (REELS) experiment follows a so-called *V*-type trajectory if it is reasonable to consider that it has only one large elastic scattering event along its total path length traveled inside the solid. *V*-type trajectories are explicitly assumed in the dielectric model developed by Yubero *et al.* [Phys. Rev. B **53**, 9728 (1996)] for quantification of electron energy losses in REELS experiments. However, the condition under which this approximation is valid has not previously been investigated explicitly quantitatively. Here, we have studied to what extent these REELS electrons can be considered to follow near *V*-type trajectories. To this end, we have made Monte Carlo simulations of trajectories for electrons traveling at different energies in different experimental geometries in solids with different elastic scattering properties. Path lengths up to three to four times the corresponding inelastic mean free paths have been considered to account for 80–90% of the total electrons having one single inelastic scattering event. On this basis, we have made detailed and systematic studies of the correlation between the distribution of path lengths, the maximum depth reached, and the fraction of all electrons that have experienced near *V*-type trajectories. These investigations show that the assumption of *V*-type trajectories for the relevant path lengths is, in general, a good approximation. In the rare cases, when the detection angle corresponds to a scattering angle with a deep minimum in the cross section, very few electrons have experienced true *V*-type trajectories. However, even in these extreme cases, a large fraction of the relevant electrons have near *V*-type trajectories.

DOI: 10.1103/PhysRevB.77.245405 PACS number(s): 79.20.Uv, 68.49.Jk

I. INTRODUCTION

It is of great technological importance to be able to study the dielectric response of ultrathin films (thicknesses of <10 nm). Reflection electron energy loss spectroscopy (REELS) is ideal for that because the probing depth for this technique is of the order of the corresponding electron inelastic mean free path λ which for 200–2000 eV electrons is $\sim 0.5-3$ nm. In order to obtain the dielectric properties of a surface by means of REELS experiments, an appropriate description of the electron energy losses of the backscattered electrons is necessary.

Quantitative analysis of the REELS spectra is a difficult task because the dielectric description of the electron energy losses in REELS experiments is a very involved problem.[1–11] Note that the backscattered electrons collected in REELS experiments do not follow a single well-defined trajectory, and the electron energy losses depend strongly on this trajectory. Excitations take place during the approach of the electron to the surface and after leaving the solid, while the electron is in the vacuum above the surface. Besides, interference effects may take place due to backscattered trajectories (induced by the field setup by the electron during the incoming trajectory on the outgoing electron).[12] In general, the boundary condition imposed by the surface on the electric field makes a rigorous model calculation very complex. This problem was treated by Yubero and co-workers,[1,2] who developed a dielectric model [Yubero–Tougaard (YT) model] that takes into account all the effects mentioned above. A theory that accounts for similar effects in photoelectron spectroscopy was later developed.[13] Many experimental tests have been presented in the past for the validity of the YT model to reproduce quantitatively the experimentally determined single inelastic scattering cross section K_{sc} (Refs. 14 and 15) (i.e., the probability for energy loss per unit path length and unit energy) or to obtain dielectric properties[16–25] of surfaces.

With the same objective, strong simplifications are taken by other authors as to consider simplified expressions for the surface electron energy losses,[26] to consider that the shape of the cross section does not depend on the kinetic energy or the surface crossing direction,[27] and thus to assume that the total excitation can be expressed as a linear combination of surface and bulk terms. Although it is possible to reproduce qualitatively REELS spectra with these approximations,[28,29] the physical information obtained from the fitting procedure is limited.[28]

Let us consider a general geometry where the electron enters the solid at the angle θ_i and exits the surface under the angle θ_o with respect to the surface normal. Inside the solid, the electron undergoes elastic and inelastic scattering events that deflect the direction of the electron and influences the distribution of total path lengths traveled by the electrons. In the YT model, there are essentially three assumptions that could influence the accuracy of their dielectric description of the electron energy losses.

(1) The results are very sensitive to the angles θ_i and θ_o of entrance and emission because they have a great influence on

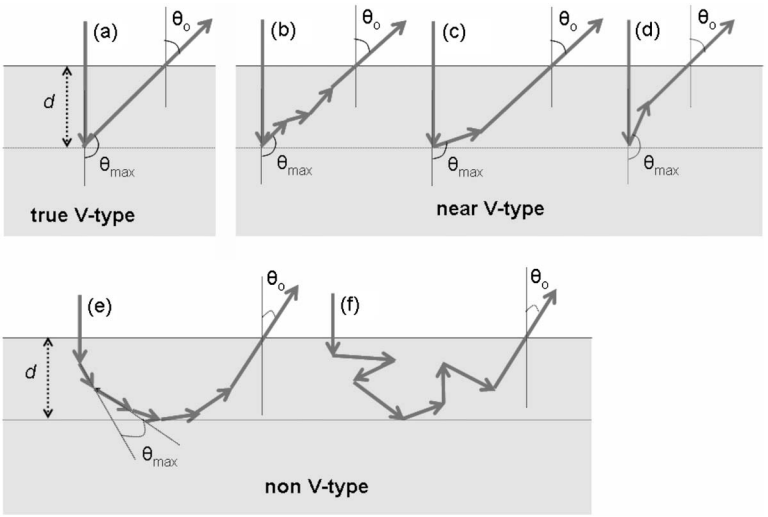

FIG. 1. Different possibilities for reflected electron trajectories: (a) true *V* type, [(b)–(d)] near *V* type, and [(e) and (f)] non-*V* type. True *V* type and near *V* type contain only one large elastic scattering angle, which is not very different from the complementary of θ_o, while non-*V* type is built either only with small elastic scattering angles or with several large scattering angles.

the relative importance of surface excitations.

(2) It is moderately dependent on the existence of *V*-type trajectories because as shown[1,2,12] there is an interference term that causes the electric field set up by the incoming electron to influence the excitation probability for the electron on its way out of the solid.

(3) The distribution of the total path lengths traveled by the electrons inside the solid before emission.

Point (1) is the most critical for the validity of the YT model. However, these angles are always exact because they are defined by the position of the electron gun and the electron detector. Points (2) and (3) are less critical for the validity of the YT model, but we may expect some dependence. It is exactly the purpose of the present paper to investigate to what extent points (2) and (3) can be assumed to be true.

As the electron travels in the solid, it will typically experience several elastic scattering events (see Fig. 1). We denote the maximum of these scattering angles as $\theta_{\max}$ and the detection angle as θ_o with respect to the surface normal. We can consider three qualitatively different types of electron trajectories for the reflected electrons as depicted in Fig. 1: (a) true *V* type, [(b)–(d)] near *V* type, and [(e) and (f)] non-*V* type. The true *V* type is characterized by a unique large angle scattering. In this case, it is fulfilled that $\theta_o = 180 - \theta_{\max}$. We define near *V*-type trajectories as those containing one large angle of scattering and several low angle scatterings that do not considerably deflect the final trajectory of the electron so that $\theta_o \approx 180 - \theta_{\max}$. Non-*V*-type trajectories are those formed either by multiple low scattering angles [Fig. 1(e)] or by several large elastic scattering angles [Fig. 1(f)]. The aim of this paper is to identify to which extent the electron trajectories in REELS experiments that contribute to the single inelastic scattering cross section can be identified as these three types of trajectories. For this purpose, we have performed Monte Carlo (MC) simulation of electron trajectories in reflected geometries considering several representative experimental conditions.

It is worth mentioning here the model developed by Oswald, Kasper, and Gaukler (OKG)[30] to describe elastic electron scattering. It takes advantage of the forward-peaked shape of the differential elastic scattering cross section and assumes that among all the elastic scattering events undertaken by the electron along its trajectory, only one of the scattering events gives rise to the total angular deflection, i.e., the OKG model approximates any electron backscattered trajectory by one true *V* type. In Ref. 31, it was shown, by comparison to extensive and systematic MC simulations, that the OKG model gives an excellent description of the angular distribution of elastically backscattered electrons in a REELS experiment. Similar results were later found.[29] This result also gives support for the validity of the *V*-type trajectory assumed in the YT model.[1,2] We can also notice the work of Vicanek[4] in which he calculates with Monte Carlo simulations the energy loss spectra for REELS and x-ray photoelectron spectroscopy (XPS). In that paper, he calculates from the invariant embedding method the path length distributions and number of elastic collision distributions for electron backscattered from different media. From his calculations, he concludes that electrons suffer a large number of small angle collisions rather than one large angle collision, a result which seems to be in contradiction with the OKG model. However, as we discuss below, this apparent contradiction originates from a difference in the physical situations simulated in the two models.

The structure of the paper is as follows. First, we identify the path lengths of interest for quantitative analysis of electron energy losses in REELS experiments. We continue with a brief description of the basis of the MC code used in this paper. In this respect, we dedicate special attention to comment on the differential elastic scattering cross section used in the MC calculations because their overall shape determines the final angular and path length distribution of backscattered electrons. Finally, we show several MC simulation tests in order to give a critical and quantitative evaluation of the trajectories undertaken by the reflected electrons that contribute to the single inelastic scattering cross sections. This allows us to test to which extent assumptions (2) and (3) above are justified.

A. Path lengths traveled by the electrons in reflection electron energy loss spectroscopy experiments

The first issue to be addressed in this study is to identify the path lengths traveled by the electrons of interest within

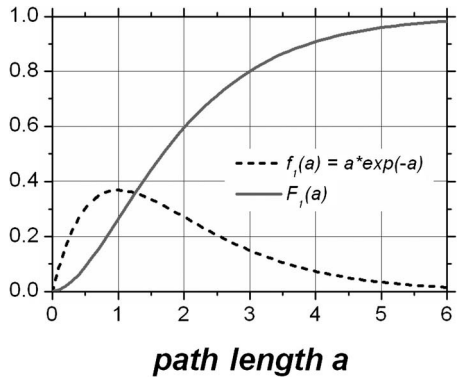

FIG. 2. Dashed line: probability density function $f_1(a)$ describing the relative amount of electrons contributing to the single inelastic scattering cross section K_{sc}. Full line: probability $F_1(a)$ that an electron that has undergone only one inelastic scattering event has traveled a reduced distance a.

the framework of quantification of the single inelastic scattering cross section from REELS experiments. We can sort the electrons detected in a REELS experiment according to the number of inelastic scattering events they have experienced. Those that are backscattered with no inelastic scattering evens, with only one inelastic scattering event, two inelastic scattering events, etc. The average total path traveled by these electrons inside the solid increases as the number of inelastic scattering events considered increases. It is well known that the inelastic scattering processes are described by the Poisson statistics. The probability that an electron experience n inelastic scattering events $f_n(a)$ after traveling a distance x inside the solid is given by the probability density function

$$f_n(a) = \frac{a^n}{n!}\exp(-a), \tag{1}$$

where $a=x/\lambda$ is the reduced distance and λ is the inelastic mean free path. Note that $n=0$ and $n=1$ correspond to the basic conditions describing the probing depth in standard analysis of elastic peak intensities in XPS and determination of the differential single inelastic scattering cross section K_{sc} in REELS, respectively. The probability that an electron that has undergone n inelastic scattering events has traveled a reduced distance a is

$$F_n(a) = \int_0^a f_n(a')da'. \tag{2}$$

Figure 2 shows the probability density function $f_1(a)$ of those electrons that contribute to the single inelastic scattering cross section as a function of the reduced distance a (dashed line). We observe that the distribution $f_1(a)$ is rather broad and that the main contribution to K_{sc} comes from electrons traveling less than three to four times λ. Figure 2 also shows $F_1(a)$, i.e., the probability that an electron that has undergone only one inelastic scattering event has traveled a reduced distance a. Note that, path lengths of up to 3λ need to be considered to account for 80% of the single inelastic scattering cross section K_{sc} in REELS.

It is interesting to compare this result to the XPS case. In XPS from a homogeneous sample, electrons are excited at all depths and consequently 80% of the contribution to the elastic peak area is achieved by considering path length of up to only 1.6λ (about half than in the REELS case to account for K_{sc}). Another difference between XPS and REELS is the kind of trajectories required to detect electrons. While in XPS usually straight-line trajectories in the solid are considered, in REELS change in the incident electron direction is required in order to have reflected trajectories. The combination of these two factors (the range of path lengths needed to explore a given depth of the material and the reflected or straight electron trajectories depending on the technique) implies that, in general, the probing depth of XPS and REELS is, to a good approximation, similar.

B. Description of the Monte Carlo simulations

We briefly describe here the basic characteristics of the MC simulation procedure used in this work. Thorough descriptions of MC simulations of electron transport can be found elsewhere in the literature.[31–35]

Classical electron trajectories are considered[33] where the electrons undergo elastic and inelastic collisions along their path in the target. These collisions are assumed to be instantaneous and the electron trajectories between two collisions are supposed to be straight lines. Typical primary kinetic energies used in REELS experiments (in the range of 200–2000 eV) have been considered. Besides, normal incidence was assumed in all the simulations performed.

A particular free path L between two collisions was sampled from the well-known formula $L=-\lambda_t \ln \beta$,[33] where β is a random number uniformly distributed between 0 and 1, $\lambda_t=\lambda\lambda_e/(\lambda+\lambda_e)$ is the total mean free path, and λ_e is the elastic mean free path. Here, λ is taken from the TPP-2M algorithm[36] and $\lambda_e=1/N\sigma_e$, where N is the atomic density of the target and σ_{el} is the total elastic scattering cross section obtained from the NIST elastic scattering database.[37] The probabilities to have elastic or inelastic collision in a given scattering event are λ_t/λ_e and λ_t/λ, respectively.

The inelastic interactions are described by λ, regardless of the energy loss produced in the inelastic collision. We are only interested in those electrons that have undergone one inelastic collision. It was assumed that the energy loss was always much smaller than the primary energy of the electron which is a good approximation for kinetic energies larger than 200 eV because the typical energy loss in a single inelastic scattering event is 10–30 eV.[38] Finally, it is assumed that the inelastic collisions do not deflect the electron trajectories.

The angular deflection of an individual elastic collision was obtained by sampling the polar angle θ between the incident electron direction and the outgoing electron direction and the azimuthal angle φ measured in the plane perpendicular to the incident electron direction. The angle θ was obtained using the differential elastic scattering cross section $d\sigma_e/d\theta$ and the angle φ was assumed uniformly distributed between 0 and 2π.

The electron trajectory is followed from the point where it penetrates into the target until it leaves the solid, or until its

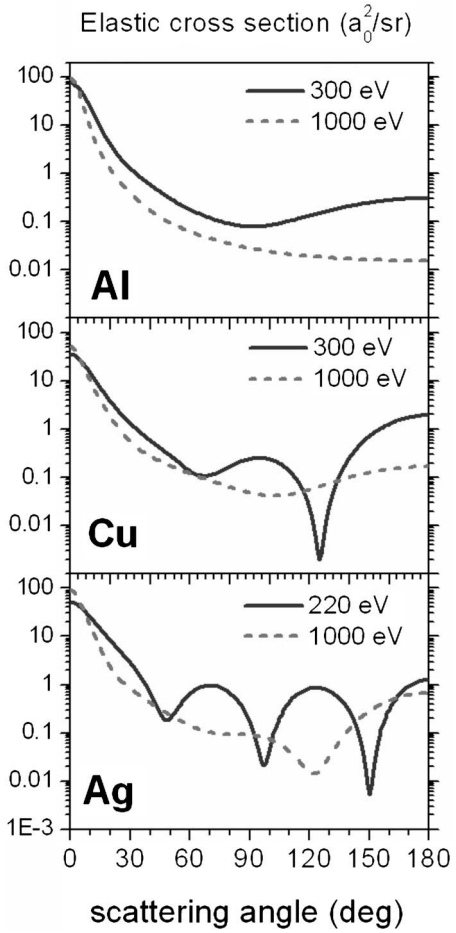

FIG. 3. Differential elastic scattering cross section versus angle of scattering (Ref. 37) for Al, Cu, and Ag evaluated at several kinetic energies.

path length gets larger than 4λ, in which case its contribution to the single differential inelastic scattering cross section is negligible.

C. Elastic scattering cross section

Elastic scattering in the MC simulations is introduced through the differential elastic scattering cross sections $d\sigma_e/d\theta$ taken from the NIST database.[37] In order to evaluate realistic cases that are representative for practical REELS experiments, several elements (Al, Cu, and Ag) and kinetic energies (220, 300, and 1000 eV) have been considered. Figure 3 shows the corresponding differential elastic scattering cross sections versus scattering angle θ. Note that forward scattering is most probable in all cases. In general, $d\sigma_e/d\theta$ decreases as the scattering angle increases and distinct structures appear as the atomic number of the scattered atoms increases. In some rare cases, sharp deep minima appear in $d\sigma_e/d\theta$, as is the case for Cu, with 300 eV and scattering angle θ=125°. Elastic scattering at this angle is very improbable and this will affect the path length distribution for the corresponding REELS geometry (see below).

D. Elastic and inelastic mean free paths

It is worth paying attention to the actual elastic and inelastic mean free paths of interest for electrons traveling in matter with 200–2000 eV. Table I shows the corresponding values used in the simulations described in this work. The number of elastic scattering events that an electron undertakes in a reflected trajectory will depend on the path length. Note that the elastic mean free paths are roughly about half of the corresponding λ. Thus, for example, if the electron path length is about 1 λ, the average number of elastic scattering events would be about 2. Taking into account (see Fig. 3) that elastic scattering angles below 10° are strongly favored (they account for ~60–90% of the probability, depending on the particular material and energy), it is then clear that the most probable trajectory in REELS would contain one large elastic scattering and another small scattering angle in the range of 0–10°. For path lengths of 2–3λ, the average number of elastic scattering events would be 4–6, which does not change the situation much (the reflected trajectory is still dominated by one large elastic scattering angle), but, in general, deviation from true *V*-type trajectories would be enhanced as the path length is increased. Besides, electron trajectories containing several large elastic scattering angles [schematically depicted in Fig. 1(f)] are of negligible importance due to the low probability for this type of events. This qualitative argument will be justified quantitatively in Secs. II and III.

TABLE I. Elastic (Ref. 37) and inelastic (Ref. 36) mean free paths used in the MC simulation of the electron trajectories described in this work

	Elastic MFP λ_e (Å)	Inelastic MFP λ (Å)
Al, 300 eV	5.8	9.8
Al, 1000 eV	13	24
Cu, 300 eV	4.8	6.8
Cu, 1000 eV	8.6	16
Ag, 220 eV	3.8	5.5
Ag, 1000 eV	7.8	15

II. RESULTS

In this section, we study the characteristics of the trajectories undertaken by the electrons participating in K_{sc} as determined in REELS experiments. This is done by a series of MC simulation tests where the relevant parameters that describe the corresponding experiment are varied systematically. Each test is designed to determine the range of validity of points (2) and (3) in Sec. I. Two conditions are required to identify how many trajectories can be considered as near *V* type to justify the approach taken in the YT model to describe electron energy losses in REELS experiments. First, as mentioned above that $\theta_{max} \approx 180 - \theta_o$, and, second, that the total path length is similar to that of a true *V*-type trajectory. Note, however, that small deviations from these conditions are not expected to be critical for the validity of the YT model.

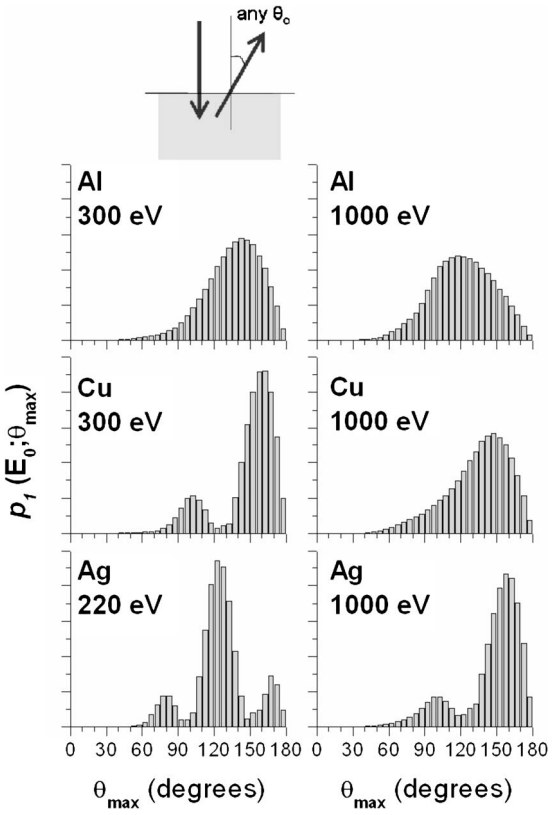

FIG. 4. Distribution of electron trajectories with only one inelastic scattering event as a function of the maximum scattering angle $\theta_{\max}$ (taking place in the total path length) for electrons incident on Al (top), Cu (middle), and Ag (bottom).

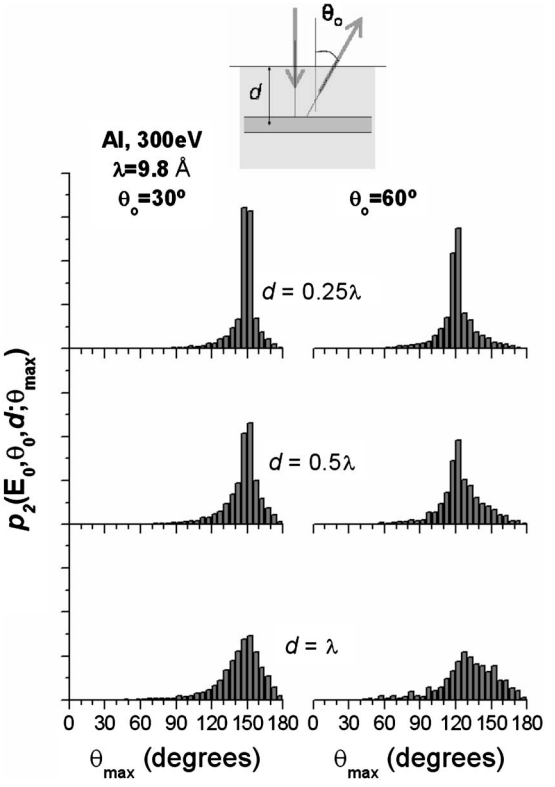

FIG. 5. Distribution of outgoing electrons with only one inelastic scattering event as a function of $\theta_{\max}$ for normal incidence, Al and 300 eV kinetic energy [λ=9.8 Å (Ref. 36)], and θ_o=30° (left) and θ_o=60° (right). Maximum depth reached by the electron d =$\lambda/4$ (top), d=$\lambda/2$ (middle), and d=λ (bottom).

Test 1: Distribution of single inelastically backscattered electrons as a function of the maximum scattering angle for normal incidence and any exit angle

In this test, we study the distribution of single inelastically backscattered electrons $p_1(E_0;\theta_{\max})$ (total path lengths of $<4\lambda$) as a function of $\theta_{\max}$ for normal incidence and varying exit angle. Figure 4 shows $p_1(E_0;\theta_{\max})$ for 300 and 1000 eV electrons impinging on the surface of Al and Cu and 220 and 1000 eV electrons on Ag. The distributions have been normalized to have the same area. Note that if $d\sigma_e/d\theta$ is featureless (as for Al at 300 and 1000 eV and Cu at 1000 eV; see Fig. 3), the distribution $p_1(E_0;\theta_{\max})$ is rather broad with a maximum between 120° and 150°. For Cu at 300 eV, the deep minimum in $d\sigma_e/d\theta$ at scattering angles θ=125° (see Fig. 3) shows up in the simulation as nearly no electrons are backscattered with $\theta_{\max}$=125° and a bimodal distribution is observed with a most probable $\theta_{\max}$ at ~160°. Qualitatively similar results are obtained for electrons backscattered on Ag for 220 eV at 150° and for 1000 eV at 120° which correspond closely to the minima in the elastic scattering cross section (see Fig. 3).

This test shows that nearly all electrons emitted after a single inelastic scattering event have undergone a large elastic scattering angle event (i.e., larger than 90°). From the data in Fig. 4, the fraction of electron trajectories that have not experienced a scattering angle larger than 90° is only 3–10% depending on the particular case. Thus, it is not probable (but possible) for the incident electrons to be reflected by several low elastic scattering angle events (which are seen in Fig. 4 as the tails for maximum scattering angles below 90°). Note that this result is obtained disregarding the depth reached by the individual electrons.

Test 2: Distribution of single inelastically backscattered electrons that have reached a given depth as a function of the maximum scattering angle for normal incidence and fixed angle of analysis

In this test, we study, for electrons of energy E_0 incident normal to the surface, the distribution $p_2(E_0,\theta_o,d;\theta_{\max})$ as a function of $\theta_{\max}$ for those electrons that are backscattered in direction θ_o (±5°) and have reached a maximum depths d (±0.2 Å) and undertaken exactly one inelastic scattering event. Note that if the electron trajectory is true *V* type [as in Fig. 1(a)], all the electrons will have $\theta_{\max}=180-\theta_o$, and if the trajectory is near *V* type [as in Figs. 1(b)–1(d)], $\theta_{\max}$ will be closely distributed around to $180-\theta_o$. Large deviations of the maximum scattering angle from $180-\theta_o$ are expected for those electrons that have non-*V*-type trajectories [as in Figs. 1(e) and 1(f)].

Figure 5 shows $p_2(E_0,\theta_o,d;\theta_{\max})$ for the case of Al with E_0=300 eV and θ_o=30° (left) or θ_o=60° (right). Maximum depths reached by the electrons of 0.25λ Å (top), 0.5λ Å (middle), and λ Å (bottom) are considered [note that λ for

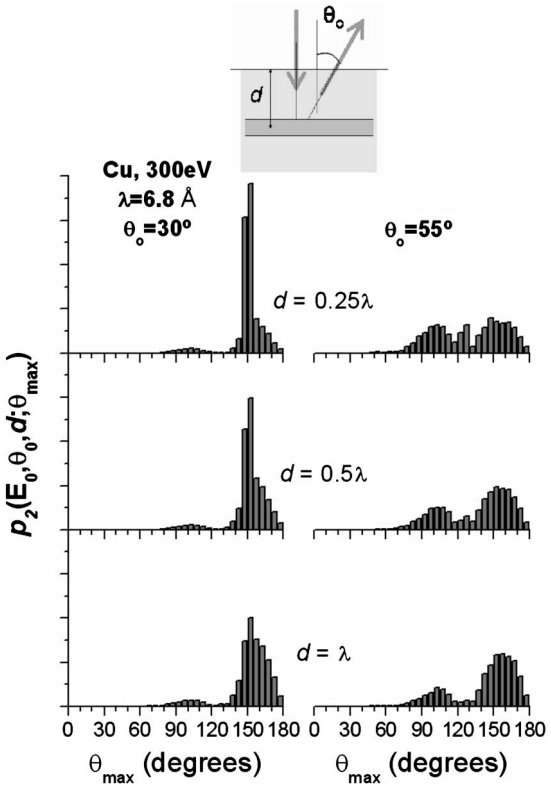

FIG. 6. Distribution of outgoing electrons with only one inelastic scattering event as a function of θ_{max} for Cu and 300 eV kinetic energy [λ=6.8 Å (Ref. 36)], normal incidence, and θ_o=30° (left) and θ_o=55° (right). Maximum depth reached by the electron d =$\lambda/4$ (top), d=$\lambda/2$ (middle), and d=λ (bottom).

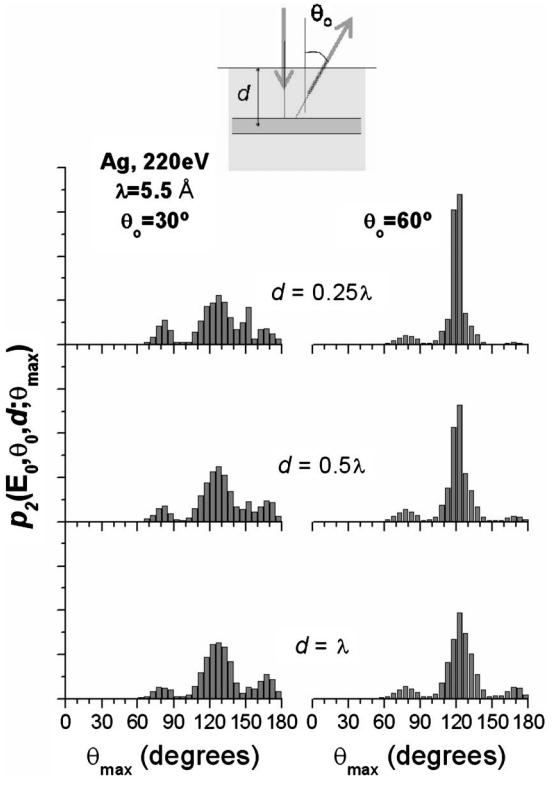

FIG. 7. Distribution of outgoing electrons with only one inelastic scattering event as a function of θ_{max} for Ag and 220 eV kinetic energy [λ=5.5 Å (Ref. 36)], normal incidence, and θ_o=30° (left) and θ_o=60° (right). Maximum depth reached by the electron d =$\lambda/4$ (top), d=$\lambda/2$ (middle), and d=λ (bottom).

300 eV electron in Al is 9.8 Å (Ref. 36)]. We observe that in all cases, the most probable maximum scattering angle θ_{max} is equal to the complementary angle of θ_o (i.e., as expected for a true V-type trajectory). This is seen for all considered values of the maximum depth d reached by the electron, although the width of the distributions increases as d increases. On the other hand, comparing the results for θ_o =30° and 60°, for larger θ_o, the p_2 distribution of θ_{max} gets broader, which implies that the deviation from true V-type trajectory gets larger although the most probable θ_{max} still correspond to a true V-type trajectory. Similar distributions were obtained for the cases of Al with E_0=1000 eV and Cu with E_0=1000 eV. In all these cases, the most probable θ_{max} coincides with the complementary angle of θ_o and the width of the distributions increases as the maximum depth reached by the electron increases. This observation points to the conclusion that, to a good approximation, the trajectories of reflected electrons contributing to K_{sc} have traveled in a near V-type trajectory, as schematically depicted in Figs. 1(b)–1(d).

Figure 6 shows $p_2(E_0,\theta_o,d;\theta_{max})$ as a function of θ_{max} for 300 eV electrons normal incident on Cu, and θ_o=30° (left) and θ_o=55° (right). Maximum depths reached by the electrons of 0.25λ Å (top), 0.5λ Å (middle), and λ Å (bottom) are considered [note that λ for 300 eV electron in Cu is 6.8 Å (Ref. 36)]. We observe that for θ_o=30°, we obtain equivalent qualitative results as those in Fig. 5. In all cases, the most probable θ_{max} is equal to that for the corresponding true V-type trajectory and the width of the distribution increases as the maximum depth reached by the electron increases. However, this is not the case for θ_o=55° (Fig. 6, right). Note that in this case, the scattering angle for a true V-type trajectory, θ_o=125°, corresponds to a deep minimum in the differential elastic scattering cross section (see Fig. 3). That is, elastic scattering with 125° is very rare. In fact, we obtain again (cf. Fig. 4) a bimodal distribution with maxima at 105° and 155°, i.e., below and above the complementary angle of 55°. Note that despite the fact that in this case the most probable θ_{max} does not match with 180−θ_o, the vast majority of trajectories of reflected electrons traveling total path lengths less than 4λ are of the near V type depicted in Figs. 1(b)–1(d), i.e., containing a large angle of scattering along their trajectory. So although we may expect that in this case true V-type trajectories are highly improbable, most electrons have near V-type trajectories containing one large scattering angle event (either about 105° or 155°) and a few small scattering angles that result in the final direction θ_o =55°.

Figure 7 shows $p_2(E_0,\theta_o,d;\theta_{max})$ as a function of θ_{max} for 220 eV electrons normal incident on Ag, and θ_o=30° (left) and θ_o=60° (right). Maximum depths reached by the electrons of 0.25λ Å (top), 0.5λ Å (middle), and λ Å (bottom) are considered [note that λ for 300 eV electron in Ag is 5.5 Å (Ref. 36)]. We observe that for θ_o=60°, we obtain

equivalent qualitative results as those described in Figs. 5 and 6 (left), i.e., the most probable $\theta_{\max}$ is equal to that for the corresponding true *V*-type trajectory and the width of the distribution increases as the maximum depth reached by the electron increases. Regarding the case $\theta_o=30°$ in Fig. 7, it is qualitatively similar to that previously described in Fig. 6 (right). Note that in this case for a true *V*-type trajectory, $\theta_{\max}=150°$ for which there is a deep minimum in the differential elastic scattering cross section (see Fig. 3). That is, elastic backscattering with 150° is very rare. In fact, we obtain again (cf. Fig. 4) a distribution with a clear maximum at 125°, i.e., well below the true *V*-type angle. Note that despite the fact that in this case the most probable $\theta_{\max}$ differs from $180-\theta_o$, the vast majority of trajectories of reflected electrons traveling total path lengths less than 4λ are of the *V*-type depicted in Figs. 1(b)–1(d), i.e., containing one large angle scattering along their trajectory. So although we expect that in this case true *V*-type trajectories are highly improbable, most electrons with $\theta_o=30°$ have near *V*-type trajectories containing a large scattering angle event of about 125° and a few small scattering angles that allow the detection at $\theta_o=30°$.

Test 3: Distribution of single inelastically backscattered electrons that have reached a given depth as a function of the total path length for normal incidence and fixed angle of analysis

In this test, we study mainly the validity of point (3) in Sec. I, concerning the distribution of path lengths. Thus, we simulate, for electrons of energy E_0 incident normal to the surface, the distribution $p_3(E_0,\theta_o,d;a)$ of path length a for those electrons that are emitted in a particular direction θ_o ($\pm 5°$), with a single inelastic scattering event along their trajectory and has reached a maximum depths d (± 0.2 Å). The obtained distributions have been normalized to have unit area.

Figure 8 shows the p_3 path length distributions for electrons traveling in Al with 300 eV (left) and Cu with 1000 eV (right) and $\theta_o=30°$ for several maximum depths d reached by the electron. All path lengths are given in units of the corresponding λ and the studied depths have been chosen as fractions of λ, i.e., $d=0.25\lambda$, 0.5λ, λ, and 1.43λ. The vertical dashed lines indicate the reduced path lengths corresponding to a true *V*-type trajectory d_V,

$$d_V=\frac{d}{\lambda}\left(1+\frac{1}{\cos\,\theta_o}\right). \tag{3}$$

We observe that these distributions are all strongly peaked at d_V. They get broader with increasing depths and the tails at large path length increase in intensity as the maximum depth is increased. Figure 8 shows that most trajectories, for this particular experimental situation, are in agreement with the expectations for true and near *V*-type trajectories depicted in Figs. 1(a) and 1(b).

Figure 9 shows p_3 path length distributions for electrons traveling in Al with 300 eV (left) and Cu with 1000 eV and $\theta_o=60°$ (right) for several maximum depths d reached by the electron. In this case, we observe that these distributions are

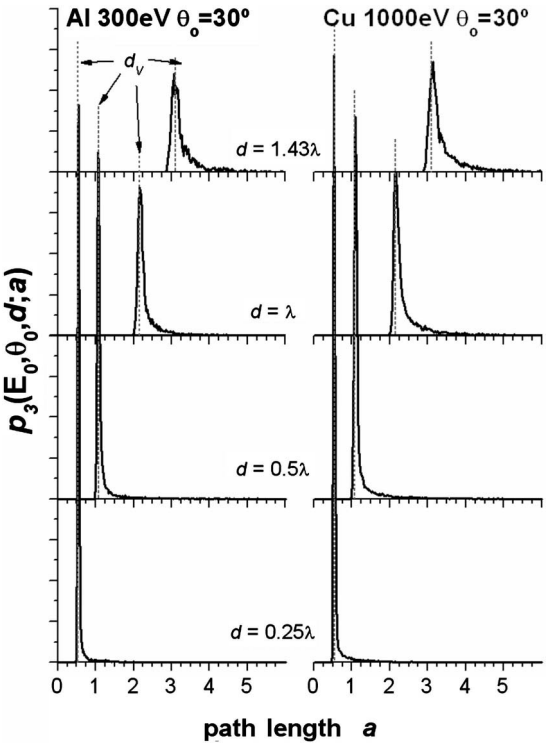

FIG. 8. Path length distributions for electrons traveling in Al with 300 eV (left) and Cu with 1000 eV (right) and $\theta_o=30°$ for several depths d reached by the electron (only one inelastic scattering event). The vertical dashed lines indicate the corresponding geometrical *V*-type path length d_V.

peaked at the corresponding d_V only for total path lengths shorter than $\sim 2\lambda$. For larger path lengths, the distributions get significantly broader, and their maxima occur at shorter path lengths than the geometrical *V*-type path length. Figure 9 shows that for $\theta_o=60°$, the path length distributions deviate significantly from the true *V*-type value for maximum depths reached by the electrons exceeding $\sim 0.5\lambda$ (i.e., total path lengths exceeding $\sim 1.5\lambda$). In these conditions, a large fraction of emitted electrons have trajectories with significantly shorter and larger path lengths than the geometrical *V*-type path length.

Figure 10 shows path length distributions for electrons traveling in Cu with 300 eV and detection angle $\theta_o=30°$ (left) and 55° (right). For $\theta_o=55°$, a true *V*-type trajectory will have a scattering angle of 125° for which there is a deep minimum in the elastic scattering cross section (see Fig. 3). Calculations are shown for several maximum depths d reached by the electron. In the case of more normal detection ($\theta_o=30°$), we observe similar behavior as in Fig. 8. For $\theta_o=55°$, the distributions are clearly peaked at the corresponding *V*-type path length for path lengths shorter than $\sim 2\lambda$, as was also the case in the examples described in Fig. 9. For larger path lengths, the distributions get broader, but their maxima are still close to the geometrical *V*-type path length. In this case, a significant amount of electron trajectories with path lengths shorter and larger than the corresponding d_V contributes to K_{sc}.

Figure 11 shows path length distributions for 220 eV electrons backscattered from Ag and emitted at $\theta_o=30°$ (left) and

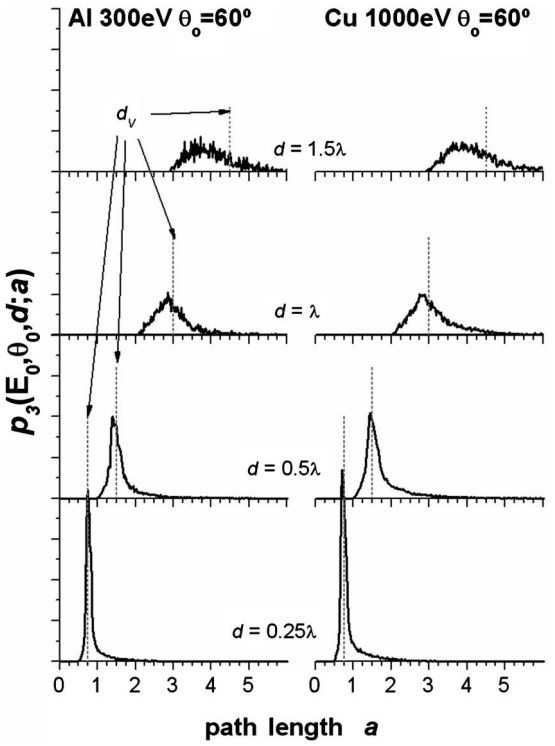

FIG. 9. Path length distributions for electrons traveling in Al with 300 eV (left) and Cu with 1000 eV (right) and $\theta_o=60°$ depicted for several depths d reached by the electron (only one inelastic scattering event). The vertical dashed lines indicate the corresponding geometrical V-type path length d_V.

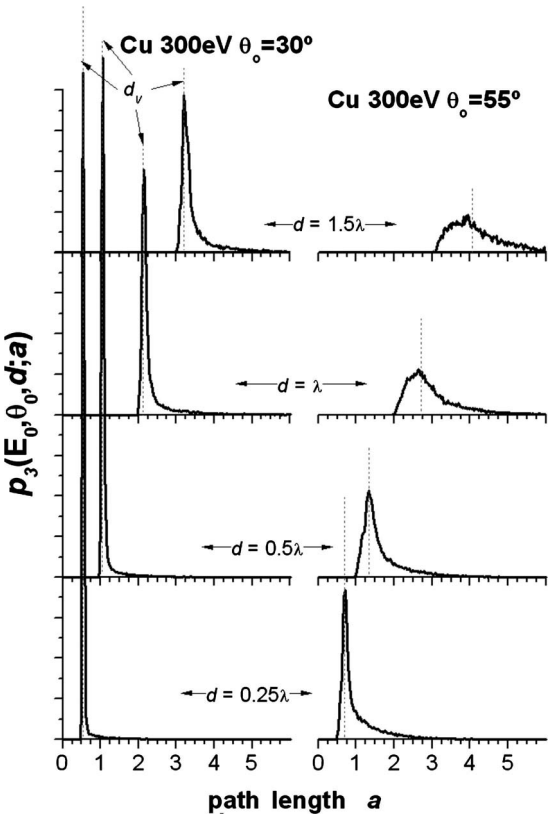

FIG. 10. Path length distributions for electrons traveling in Cu with 300 eV and $\theta_o=30°$ (left) and $\theta_o=55°$ (right) depicted for several depths d reached by the electron (only one inelastic scattering event). The vertical dashed lines indicate the corresponding geometrical V-type path length d_V.

60° (right). Calculations are shown for several maximum depths d reached by the electron. In the case of more normal detection ($\theta_o=30°$), a true V-type trajectory will have a scattering angle of 150° for which there is a deep minimum in the elastic scattering cross section (see Fig. 3). We observe similar behavior to that described in Fig. 8, but with wider distributions even for the most shallow trajectories and longer tails for the path lengths larger than those corresponding to true V-type trajectories. In the case of more glancing detection ($\theta_o=60°$), the distributions are similar to those described in Fig. 9.

III. DISCUSSION

We will now discuss assumption (2) for the YT model mentioned in Sec. I. According to the MC simulations described above, we expect deviation from true V-type trajectories due to the three effects: the large probability for small angle elastic scattering, the glancing detection (and probably also glancing incidence), and the special geometries where the complementary angle of θ_o coincides with a deep minimum in the $d\sigma_e/d\theta$.

The large probability for small angle elastic scattering results in a broadening of the $\theta_{\max}$ and path length distributions only for path lengths larger than $2-3\lambda$. This is clearly seen in Figs. 5–11.

Figures 5–7 show $\theta_{\max}$ distributions of reflected electrons with a single inelastic scattering event along their trajectory that have reached a given depth. In most cases, the most probable $\theta_{\max}\approx 180-\theta_o$, suggesting that near V-type trajectories are most probable. The percentage of trajectories for which $180-\theta_o$ differs from the most probable $\theta_{\max}$ by less than 15° can be calculated as

$$P_2(\%) = \int_{\theta_o-15°}^{\theta_o+15°} p_2(E_0,\theta_o,d;\theta_{\max})d\theta_{\max}. \quad (4)$$

Figure 12 shows $P_2(\%)$ for different θ_0 and d as a function of the corresponding d_V. We observe that for 70–80% of all trajectories, the most probable $\theta_{\max}=(180-\theta_0)\pm 15°$ for $\theta_o=30°$. This percentage diminishes to 50–70% for $\theta_o=60°$ depending on the particular experimental conditions. Only for the special cases where the complementary of the exit angle coincides with a deep minimum in the elastic cross section (as, for example, Cu at 300 eV, $\theta_o=55°$ and Ag at 220 eV, $\theta_o=30°$), the fraction of electron trajectories for which the most probable $\theta_{\max}=(180-\theta_0)\pm 15°$ decreases to about 30%. Note that also in these latter cases, the electron trajectories contain one large scattering angle that is close to the expected angle for true V-type trajectories, so trajectories as those depicted in Figs. 1(c) and 1(d) are mostly expected. This, together with the estimate made above, that the average number of elastic scattering events, expected for each electron trajectory contributing to K_{sc}, is 4–6, suggests that the

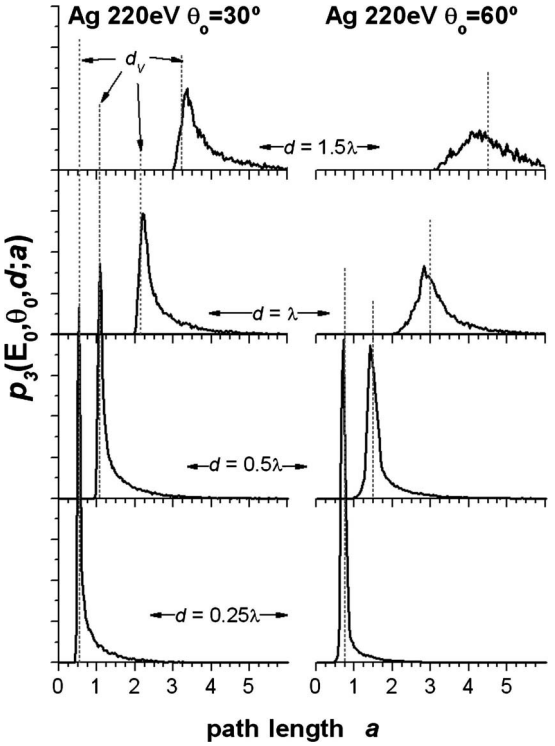

FIG. 11. Path length distributions for electrons traveling in Ag with 220 eV and $\theta_o=30°$ (left) and $\theta_o=60°$ (right) depicted for several depths d reached by the electron (only one inelastic scattering event). The vertical dashed lines indicate the corresponding geometrical *V*-type path length d_V.

most probable electron trajectory even for these special geometries will consist of one large scattering angle and a few (one to six) small scattering angle of about 1–20° that allow the electron to be detected at the angle θ_o and that the $\theta_{\max}$ angle deviates from the true *V*-type angle by 20–30° (see the bimodal structure of the distributions).

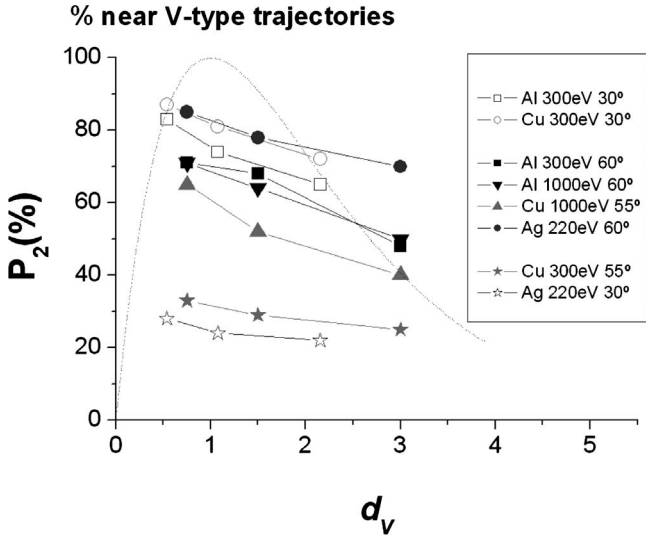

FIG. 12. Percentages $P_2(\%)$ of near *V*-type trajectories for different experimental situations (see legend) as defined in the text. Also included a function proportional to $f_1(a)$ (dashed line) for comparison of the relative importance of each path length for K_{sc}.

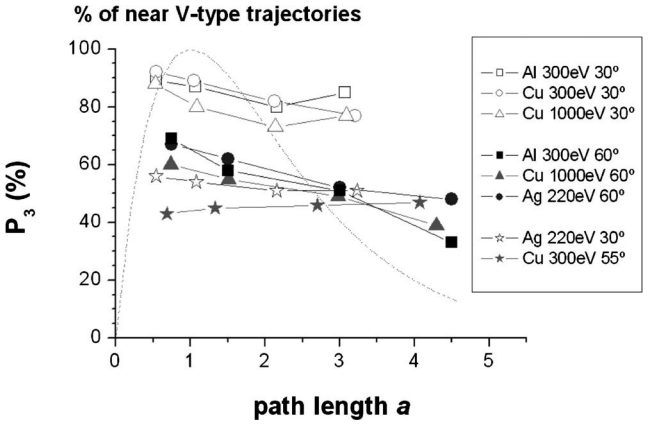

FIG. 13. Percentages $P_3(\%)$ of near *V*-type trajectories for different experimental situations (see legend) as defined in the text. Also included a function proportional to $f_1(a)$ (dashed line) for comparison of the relative importance of each path length for K_{sc}.

Figures 8–11 show path length distributions of reflected electrons with a single inelastic scattering event along their trajectory that has reached a given depth. The probability to find an electron trajectory with a path length within 10% of the true *V*-type trajectory d_V is

$$P_3(\%) = \int_{d_V-10\%}^{d_V+10\%} p_3(E_{0,}\theta_o,d;a)da. \tag{5}$$

The result is plotted in Fig. 13.

For $\theta_o=30°$ and when there is no singularity in $d\sigma_e/d\theta$ at 150° [as in Figs. 8 and 10 (left)], narrow path length distributions are obtained, which are peaked at the corresponding d_V. Only for depths reached by the electrons larger than 1.5λ, the distributions start to get broader mainly on the right side of the peaks, indicating that the fraction of path lengths larger than d_V is enhanced. As seen in Fig. 13, in this case, 80–90% of the total number of electron trajectories have path lengths that deviate <10% from the true *V*-type trajectory [i.e., they have paths as depicted in Figs. 1(a) and 1(b)].

For $\theta_o=60°$ and no singularity in $d\sigma_e/d\theta$ [as in Figs. 9 and 11 (right)], narrow path length distributions, peaked at the corresponding d_V, are obtained only for depths less than 0.5λ. For larger depths reached by the electrons, the path length distributions get broader and the fraction of trajectories with path lengths shorter than the corresponding d_V is enhanced. The origin of this behavior is that the corresponding p_1 distributions in Fig. 4 are broad functions with maximum at 140°–150° (note that for $\theta_o=60°$, the corresponding $\theta_{\max}$ for a true *V*-type trajectory is 120°). As larger path lengths are considered, the most probable $\theta_{\max}$ obtained in the p_1 distributions will start to show up, thus the electron trajectory will consist of one large scattering angle around 140°–150° and a few small scattering angles to let the electron be detected with $\theta_o=60°$. Since this angle is larger than the scattering angle for a true *V*-type trajectory, this tends to shorten the total path length slightly [as in Fig. 1(d)] in accordance with the distributions for $\theta_o \sim 60°$ in Figs. 8–11. As seen in Fig. 13, in this case, 60–65% of the total number of electrons have path lengths that deviate less than 10% from

that of a true *V*-type trajectory and their trajectories can be considered as near *V* type [as depicted in Fig. 1(b)]. Besides, an important amount of the remaining 35–40% of the trajectories also is of the near *V* type as those depicted in Fig. 1(d), for which the total path length is shorter than the corresponding d_V.

The cases when the complementary angle of θ_o coincides with a deep minimum in the elastic scattering cross section require special attention. In practice, these situations may appear for materials with high atomic number and low kinetic energy of the impinging electrons. In the particular case of detection angles near normal to the surface (as, for example, Ag at 220 eV and $\theta_o=30°$), small deviations from the situation described above for the same detection angle and no singularity in the elastic cross section are observed. The distributions are still peaked at the corresponding d_V. However, they are broader than the corresponding distributions without singularity in the elastic cross section [compare Fig. 11 (left) and Fig. 8]. Besides, path lengths larger than d_V are significantly enhanced for even the shortest depths reached by the electrons. In this case, as the scattering angle of 150° is strongly handicapped by the elastic cross section, the electrons to be detected in reflection mode at $\theta_o=30°$ will be scattered mostly with scattering angles of about 120° (see p_1 distributions depicted in Fig. 4 and p_2 distribution in Fig. 7), and as a consequence, larger path lengths will take place with significant amount.

On the other hand, if $(180°-\theta_o)$ coincides with a deep minimum in the elastic scattering cross section for more glancing detection (as for $\theta_o=55°$ with 300 eV electrons on Cu), the resulting path length distributions are not very different from that described above for $\theta_o=60°$ without a singularity in the elastic cross section. The only remarkable effect is that for shallow trajectories, broader distribution is observed and shorter path lengths than d_V are enhanced. This can be justified noting again that the corresponding p_1 distribution depicted in Fig. 4 and p_2 distribution in Fig. 6 have a maximum of about 160°, thus trajectories of the type shown in Fig. 1(d) will be enhanced. In these cases, 45–55% of the trajectories can be strictly considered as near *V* type, as those depicted in Fig. 1(b), according to the definition in Eq. (5). Besides, an important amount of the remaining trajectories would also be of the near *V* type as those depicted in Fig. 1(d), for which the total path length is shorter than the corresponding d_V.

Summarizing, we have found that for most experimental situations, the majority of the electrons have traveled a total distance that is close to that for a true *V*-type trajectory. Besides, it is found that, to a good approximation, the most probable $\theta_{\max}$ is approximately $180-\theta_0$. Moreover, even in cases where this latter condition is not satisfied, the vast majority of the electrons have experienced one large scattering angle (>90°), and thus these electron trajectories are also near *V* type as those depicted in Figs. 1(c) and 1(d), while the trajectories in Figs. 1(e) and 1(f) are extremely rare in all cases.

Thus, in general, when $180°-\theta_o$ does not coincide with a deep minimum in the elastic scattering cross section and for nonglancing detection angles (represented by $\theta_o=30°$ in the examples described in this paper), it is found that more than 80% of the total amount of electrons participating in the single inelastic scattering cross section follow near *V*-type trajectories. For more glancing detection (represented by $\theta_o=60°$ in the examples described in this paper), the fraction of near *V*-type trajectories decreases to about 60% of the total amount of trajectories contributing to K_{sc}. In this latter case, the fraction of electrons with path lengths shorter that the corresponding *V*-type is enhanced (see Fig. 9). On the other hand, for the special cases, when $180°-\theta_o$ coincide with a deep minimum in the elastic scattering cross section, deviations are observed, so larger path lengths are enhanced for near normal emission (i.e., $\theta_o=30°$) while shorter path lengths are enhanced for more glancing emission angles (i.e., $\theta_o=60°$). As a consequence, at least 45–55% of the total number of trajectories can still be considered as near *V* type even in these cases.

Here, it is worth stressing that despite of the fact that 20–40% of electron trajectories cannot be strictly considered as near *V* type, the inelastic scattering cross section K_{sc}, evaluated according to the YT model,[1,2] closely reproduces experimental findings for a wide range of energies, materials, and geometries.[14,15] This suggests that this model gives a good description of the energy loss processes and that the averaging over larger and shorter path lengths as well as over larger and smaller elastic scattering deflections around the most probable $\theta_{\max}$ compensate in the experimental REELS trajectories, in a similar manner to the averaging performed over the path lengths [given by Eq. (1)] for a fixed scattering angle within the YT model.

At first glance, it might seem that our results are in contradiction to those of Vicanek[4] who concludes that backscattered electrons have suffered a large number of collisions. However, this is no contradiction because the range of trajectories he studies is totally different from ours. Thus, in his calculations, Vicanek[4] considers all electron trajectories including those with large path lengths which will indeed typically have suffered a large number of elastic and inelastic interactions before they escape. The purpose of our simulations is, however, to study the electron trajectories that contribute to that part of the REELS spectrum where electrons have suffered only one inelastic collision or with a total path length of $<4\lambda$.

IV. SUMMARY AND CONCLUSIONS

The electron trajectories of reflected electrons in REELS experiments that contribute to the single inelastic scattering cross section can be considered in most cases, to a good approximation, as true and near *V* type [cf. Figs. 1(a)–1(d)]. Thus, about 80% of the total amount of electron trajectories for normal incidence and detection angles about 30° can be considered as near *V* type (mainly type *b* in Fig. 1). The percentage of near *V*-type trajectories decreases to about 60% when more glancing ($\theta_o=60°$) trajectories are considered. A special situation occurs when a detection angle is chosen so that the corresponding *V*-type scattering angle coincides with a deep minimum in the differential elastic

scattering cross section. In such cases, most of the electron trajectories contributing to K_{sc} will be of types c and d depicted in Fig. 1, while the trajectories in Figs. 1(e) and 1(f) are improbable even for these extreme cases.

ACKNOWLEDGMENT

S.T. acknowledges financial support from the Danish Natural Science Research Council (FNU).

[1] F. Yubero and S. Tougaard, Phys. Rev. B **46**, 2486 (1992).
[2] F. Yubero, J. M. Sanz, B. Ramskov, and S. Tougaard, Phys. Rev. B **53**, 9719 (1996).
[3] A. L. Tofterup, Phys. Rev. B **32**, 2808 (1985).
[4] M. Vicanek, Surf. Sci. **440**, 1 (1999).
[5] Z.-J. Ding and R. Shimizu, Phys. Rev. B **61**, 14128 (2000).
[6] A. Jablonski, Prog. Surf. Sci. **74**, 357 (2003).
[7] L. G. Glazov and S. Tougaard, Phys. Rev. B **68**, 155409 (2003).
[8] L. G. Glazov and S. Tougaard, Phys. Rev. B **72**, 085406 (2005).
[9] W. S. M. Werner, Phys. Rev. B **74**, 075421 (2006).
[10] T. Nagatomi and K. Goto, Phys. Rev. B **75**, 235424 (2007).
[11] L. Calliari, M. Dapor, and M. Filippi, Surf. Sci. **601**, 2270 (2007).
[12] N. Pauly, S. Tougaard, and F. Yubero, Phys. Rev. B **73**, 035402 (2006).
[13] A. Cohen Simonsen, F. Yubero, and S. Tougaard, Phys. Rev. B **56**, 1612 (1997).
[14] F. Yubero, D. Fujita, B. Ramskov, and S. Tougaard, Phys. Rev. B **53**, 9728 (1996).
[15] S. Hajati, O. Romanyuk, J. Zemek, and S. Tougaard, Phys. Rev. B **77**, 155403 (2008).
[16] F. Yubero, S. Tougaard, E. Elizalde, and J. M. Sanz, Surf. Interface Anal. **20**, 719 (1993).
[17] F. Yubero, J. M. Sanz, J. F. Trigo, E. Elizalde, and S. Tougaard, Surf. Interface Anal. **22**, 124 (1994).
[18] F. Yubero, J. P. Espinós, and A. R. González-Elipe, J. Vac. Sci. Technol. A **16**, 2287 (1998).
[19] P. Prieto, F. Yubero, E. Elizalde, and J. M. Sanz, J. Vac. Sci. Technol. A **14**, 3181 (1996).
[20] H. Jin, S. K. Oh, H. J. Kang, and S. Tougaard, J. Appl. Phys. **100**, 083713 (2006).
[21] H. Jin, S. K. Oh, Y. Joon Cho, H. J. Kang, and S. Tougaard, J. Appl. Phys. **102**, 053709 (2007).
[22] P. Prieto, C. Quirós, E. Elizalde, and J. M. Sanz, J. Vac. Sci. Technol. A **24**, 396 (2006).
[23] W. de la Cruz, G. Soto, and F. Yubero, Opt. Mater. **25**, 39 (2004).
[24] G. G. Fuentes, I. G. Mancheño, F. Balbas, C. Quiros, J. F. Trigo, F. Yubero, E. Elizalde, and J. M. Sanz, Phys. Status Solidi A **175**, 429 (1999).
[25] P. Prieto, S. Hofmann, E. Elizalde, and J. M. Sanz, Surf. Interface Anal. **36**, 1392 (2004).
[26] C. J. Tung, Y. F. Chen, C. M. Kwei, and T. L. Chou, Phys. Rev. B **49**, 16684 (1994).
[27] W. S. M. Werner, Surf. Sci. **588**, 26 (2005).
[28] F. Yubero and S. Tougaard, Surf. Interface Anal. **19**, 269 (1992).
[29] W. S. M. Werner, Phys. Rev. B **71**, 115415 (2005).
[30] R. Oswald, E. Kasper, and K. H. Gaukler, J. Electron Spectrosc. Relat. Phenom. **61**, 251 (1993).
[31] A. Dubus, A. Jablonski, and S. Tougaard, Prog. Surf. Sci. **63**, 135 (2000).
[32] M. H. Kalos and P. A. Whitlock, *Monte Carlo Methods: Basics* (Wiley, New York, 1986), Vol. 1.
[33] R. Shimizu and Ding Ze-Jun, Rep. Prog. Phys. **55**, 487 (1992).
[34] A. Dubus, M. Rösler, and O. Benka, Math. Comput. Simul. **55**, 37 (2001).
[35] A. Jablonski, C. J. Powell, and S. Tanuma, Surf. Interface Anal. **37**, 861 (2005).
[36] S. Tanuma, C. J. Powell, and D. R. Penn, Surf. Interface Anal. **21**, 165 (1993).
[37] Standard Reference Data Program 64, Electron-Elastic-Scattering Cross-Sections Database Version 3.1, National Institute of Standards and Technology, Gaithersburg, 2003.
[38] S. Tougaard, Surf. Interface Anal. **25**, 137 (1997).